ACS OMEGA

Open Access

http://pubs.acs.org/journal/acsodf

Article

Molecular and Energetic Descriptions of the Plasma Protein Adsorption onto the PVC Surface: Implications for Biocompatibility in Medical Devices

Amr H. Saleh, Ghazal Borhan, Florent Goujon, Julien Devémy, Alain Dequidt, Patrice Malfreyt,* and Mehdi Sahihi*

Cite This: *ACS Omega* 2024, 9, 38054−38065

Read Online

ACCESS | Metrics & More | Article Recommendations | Supporting Information

ABSTRACT: Protein adsorption on material surfaces plays a key role in the biocompatibility of medical devices. Therefore, understanding the complex interplay of physicochemical factors driving this kind of biofouling is paramount for advancing biomaterial design. In this study, we investigated the interaction of the most prominent plasma proteins with polyvinyl chloride (PVC) as one of the ubiquitous materials in medical devices. Through molecular docking, we identified human serum albumin (HSA) as a plasma protein with the highest affinity for adsorption onto the PVC surface with the binding energy of −25.9 kJ mol^{-1}. Subsequently, utilizing triplicate molecular dynamics (MD) simulations (0.5 μs each), we quantitatively analyzed the interactions between HSA and PVC, probing potential structural changes in the protein upon adsorption. Our findings revealed that water-mediated hydrogen bonds and van der Waals forces are key contributors in stabilizing HSA onto the surface of PVC without significant alteration to its secondary and tertiary structures. The observed distribution of water molecules further highlights the importance of the hydration layer in facilitating and modulating protein−polymer interactions. We further evaluated the thermodynamic properties governing the adsorption process by calculating the potential of mean force (PMF) along the direction normal to the surface. The computed Gibbs free energy of adsorption at 300 K (−507.4 kJ/mol) indicated a thermodynamically favored and spontaneous process. Moreover, our investigations across different temperatures (290 to 310 K) consistently showed an enthalpy-driven adsorption process.

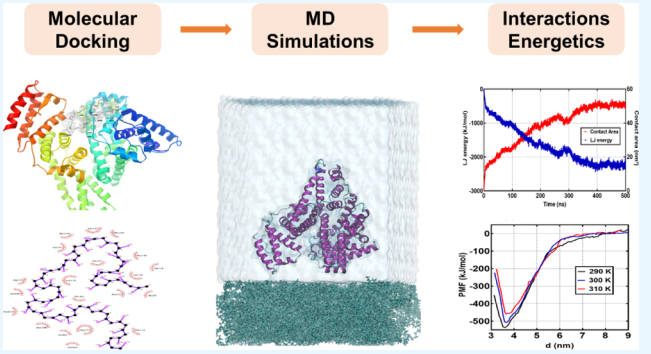

1. INTRODUCTION

The interface between biological systems and synthetic materials has long been a topic of critical importance in various fields of science and medicine. When it comes to medical devices implanted in the human body, the interaction between blood and foreign surfaces initiates a complex process known as plasma protein adsorption, which significantly influences subsequent blood-material interactions.[1,2] This phenomenon, also known as biofouling, involves the spontaneous adsorption of proteins and other biomolecules on surfaces.[3] Biofouling facilitates the accumulation and adhesion of various cell types[4] and emerges as a critical factor affecting biocompatibility. Such interactions may lead to complications like infections and device malfunctions, attributed to the formation of bacterial biofilms on the adhered protein layer.[5] The trifecta of protein adsorption, biofilm formation, and ensuing complications poses a significant challenge in the biomedical industry, incurring substantial economic costs, amounting to billions of US dollars annually in the United States alone.[6]

A comprehensive understanding of the interface between human plasma and polymers is crucial for advancing biomaterial science. Transitioning from a paradigm where predictable performance is rare to one where it is the standard necessitates refined processing and selection criteria for materials in final clinical products.[7] This shift in focus, from bulk to interfacial properties as pivotal determinants in medical device outcomes, has spurred diversified research efforts. Researchers are delving into the intricacies of physicochemical and cell-mediated processes at artificial surfaces, aiming to establish fundamental guidelines for optimizing performance.[8−10]

Received: May 29, 2024
Revised: August 1, 2024
Accepted: August 12, 2024
Published: August 26, 2024

Developing more targeted recommendations and efficient anti/nonbiofouling strategies, along with creating surfaces or textiles with improved resistance to biofouling, becomes achievable with a deeper understanding of the physicochemical aspects of interactions between biomolecules (especially proteins) and materials. Plasma protein adsorption emerges as a key indicator for enhancing blood compatibility, driving multifaceted studies investigating surface properties such as coverage, conformation, orientation, kinetics, exchange, desorption, and intermolecular interactions across a range of materials.[11,12]

Polyvinyl chloride (PVC), one of the most prevalent polymers in medical devices and a leading thermoplastic material, is expected to surpass a global production volume of 60 million metric tons by 2025.[13,14] The commendable properties of PVC, such as its low manufacturing cost, lightweight nature, and recyclability, make it indispensable across diverse sectors, particularly in medical devices.[15,16] Nevertheless, a comprehensive understanding of the interactions between PVC and blood components remains elusive.

Prominent plasma proteins, selected based on their physiological significance, presence in blood, and potential to interact with foreign surfaces, include: (i) Human Serum Albumin (HSA), constituting 60% of plasma proteins with a molecular weight of 66.5 kDa. HSA plays a pivotal role in maintaining osmotic pressure and transporting substances such as hormones, fatty acids, and drugs, highlighting its relevance. Notably, HSA exhibits a robust adsorption capacity on various surfaces, including synthetic materials like PVC.[17,18] (ii) Fibrinogen (FB), a protein of 340 kDa central to blood clotting, is of interest due to its affinity for adsorption onto PVC surfaces.[19,20] (iii) Human Transferrin (HTR), an 80 kDa glycosylated protein integral to iron homeostasis. Besides its role in iron regulation, HTR's potential bacteriostatic effects may influence biofilm-forming microorganisms,[21,22] and (iv) C3b Protein, a component of the complement system pivotal in immune response, particularly opsonization, marking pathogens for immune cell destruction.[23−25]

Current experimental methods to counteract biofouling in PVC-based medical devices either pose risks or demonstrate limited efficacy.[26−28] Hence, advancing strategies to mitigate bio/nonbiofouling requires a fundamental grasp of the physicochemical dynamics between plasma proteins and PVC. Conventional experimental techniques, such as X-ray photoelectron spectroscopy (XPS) or electron microscopy, provide valuable insights but are limited in accurately simulating real-world conditions.[29] These methods operate in vacuum conditions, deviating from the actual environment where protein-biomaterial interactions occur.[30] Therefore, there is a pressing need to complement experimental approaches with computational techniques such as molecular modeling and simulations.[31] Computational methods offer precise predictions at the molecular level, filling in gaps in our understanding of macromolecular properties observed experimentally.[32] Atomistic molecular dynamics (MD) simulations, leveraging recent advancements in computing power, enable the scrutiny of systems over time scales ranging from subnanoseconds to microseconds.[33] Previous studies have highlighted the utility of MD simulations in investigating protein adsorption on various biomaterials.[34−40] Investigating protein adsorption onto a polymeric material's surface through molecular methods proves challenging due to the large system size, heterogeneous surface, and structural flexibility of the adsorbate, necessitating extended simulation times to achieve system relaxation. Conversely, the computation of adsorption free energy presents a more formidable challenge due to the multitude of degrees of freedom requiring sampling. Recent work in our research group addressed the calculation of adsorption free energy for the insulin-PVC complex,[41] laying the groundwork for extending this approach to the demanding calculation of adsorption free energy for plasma protein adsorption onto PVC surfaces.

Therefore, the objective of this study is to investigate the fundamental physicochemical aspects of interactions between plasma proteins and PVC, one of the most commonly used polymers in medical devices. The aim is to identify the factors that render PVC-based medical devices prone to plasma proteins. This study employs diverse computational techniques to probe this process.

Beginning with a molecular docking experiment to ensure appropriate initial protein orientation—an essential factor influencing adhesion energy and protein−polymer interactions.[42] This experiment not only scores plasma proteins based on their affinity for PVC surface adsorption but also serves as a cost-effective means to ascertain protein orientation on PVC surfaces.[43,44] Subsequent parallel molecular dynamics (MD) simulations of proteins in water and protein adsorption onto PVC surfaces allow for an in-depth exploration of protein structure and behavior during the adsorption process.

It is anticipated that the insights gleaned from this comprehensive study, which delves into the adsorption of plasma proteins onto PVC-based medical devices, encompassing the intricate calculation of adsorption free energy and examining changes in protein structure and hydration properties relative to bulk water conditions, will illuminate the path toward designing and developing a new generation of biomedical materials with heightened biocompatibility and anti/nonbiofouling properties.

2. COMPUTATIONAL PROCEDURES

2.1. Molecular Docking. In this study, molecular docking was employed to investigate the binding interactions between a PVC chain and major human serum proteins, namely HSA, FB, C3b, and HTR. The aim was to determine the most favorable binding sites and orientations on the PVC surface. Polymeric surfaces cannot be used in docking studies, however several research groups have shown that using a model chain of the polymer of interest is suitable and can be representative of the polymer surface.[45−47] Hence, one PVC chain was modeled as a ligand using GaussView[48] and Gaussian16[49] software, applying the PM6 semiempirical method. The 35-mer PVC chain served as the ligand model, while crystallographic structures of HSA (PDB code: 1AO6), FB (PDB code: 3GHG), C3b (PDB code: 5FO8), and HTR (PDB code: 3 V83) were selected as model templates.

Prior to docking, protein structures were processed by removing water molecules and determining missing side chains and the protonation state of histidine residues using the WHATIF web interface.[50] Gasteiger charges were assigned to the macromolecule for the docking procedure using AutoDock Vina.[51,52] The analysis of ligand-protein interactions, along with the determination of intermolecular energies, provided insights into the binding preferences between PVC and the selected proteins. A 2D diagram illustrating amino acids involved in these interactions was generated using *Ligplot*$^{+}$ V.2.2.8.[53]

https://doi.org/10.1021/acsomega.4c05044
ACS Omega 2024, 9, 38054−38065

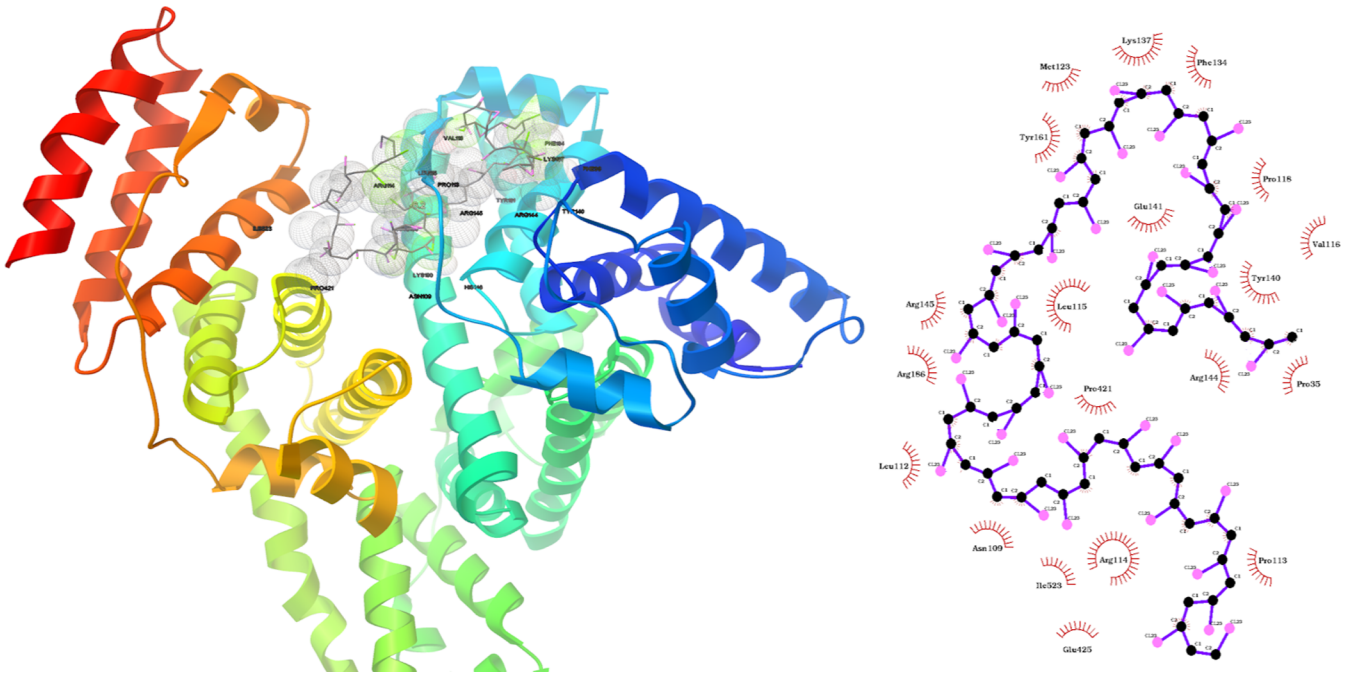

Figure 1. 2D and 3D molecular docking maps showing molecular interactions between PVC chain with HSA protein. Hydrophobic interactions are shown by red arcs.

2.2. MD Simulations. We established a molecular system with a protein in a water box, positioned atop a PVC slab previously prepared. The PVC slab, measuring 10 × 10 × 5 nm^3, comprised 171 PVC chains, resulting in a PVC density of approximately 1.24 g cm^{-3}, closely matching the reported experimental value of 1.40 g cm^{-3} for amorphous PVC.[54] The PVC chains were parametrized using the CHARMM36 force field, known for its success in modeling PVC samples.[55]

For the amorphous PVC slab, equilibrated PVC chains underwent a heating−cooling procedure (300 K-1000 K-300 K) at a rate of 50 K ns^{-1}. The starting conformation of the MD simulation was based on docking results. The PVC slab was positioned at the bottom of the simulation box, with the protein positioned approximately 0.5 nm above the PVC slab. A 5 nm vacuum layer was added on top to prevent interactions with the periodic boundary image of PVC, resulting in a final system size of 10 × 10 × 19 nm^3. As a reference, another system containing only the protein in a water box without the PVC slab was prepared in a cubic box measuring 11.4 × 11.4 × 11.4 nm^3.

Both systems were neutralized with Na^+ and Cl^- ions to achieve a concentration of 150 mM, with approximately 40,000 water molecules surrounding the protein. The composition of the two simulation systems is illustrated in Figure S1 of the Supporting Information.

All MD simulations were performed using the GROMACS 2021.6 simulation package.[56−59] The CHARMM36 force field, validated for protein−polymer interactions,[39] was employed. A time step of 1.0 fs was used, employing XYZ periodic boundary conditions. The systems underwent energy minimization using the Conjugate Gradient (CG) method, with convergence criteria set at 1 × 10^{-6} kJ mol^{-1} for energy difference and 1 × 10^{-6} kJ mol^{-1} nm^{-1} for RMS force. Subsequently, a 0.5 μs NVT production run was conducted at 300 K, using a Nose-Hoover thermostat with a damping constant of 0.2 ps. Lennard-Jones and Coulomb interactions had a cutoff of 1.0 nm, and the particle mesh-Ewald (PME) method and LINCS algorithm handled long-range electrostatics and constraints, respectively. The MD simulation of protein-PVC system was performed in triplicates (0.5 μs each), all results are represented as the average values of these triplicate MD simulations. Visualization and analyses were performed using VMD software V.1.9.3[60] and GROMACS 2021.6.

2.3. Potential of Mean Force (PMF) Calculations. To quantify the adsorption energy of the protein on the PVC surface, we performed PMF calculations. The last configuration of the MD simulation, at equilibrium, served as the starting point for steered MD (SMD) simulations, during which we applied a force along the z dimension of the simulation box. A spring constant of 4000 kJ mol^{-1} nm^{-2} and a pull rate of 0.01 nm ps^{-1} were chosen for the 1 ns pulling simulation.

Configurations for umbrella sampling (US) were generated with a spacing window of 0.08 and a total distance of 7 nm between the center of mass of the protein and the PVC slab. This resulted in 89 configurations along the protein-PVC reaction coordinate (the z dimension). Each umbrella sampling window underwent a 1 ns equilibration and a subsequent 5 ns NVT production run with a 4000 kJ mol^{-1} nm^{-2} umbrella potential. The Gibbs free energy profile along the reaction path was constructed using the Weighted Histogram Analysis Method (WHAM), integrated into GROMACS as the WHAM module.[61]

To explore the temperature dependence of the adsorption process, we repeated PMF calculations at 290 and 310 K, too. The last MD configuration underwent a 10 ns equilibration (at the new temperature) before PMF calculations with the previously mentioned parameters. To analyze the thermodynamic properties, we employed the Gibbs−Helmholtz equations[62] (eqs 1 and 2). Plotting $\Delta_r G^o$ against temperature allowed us to determine the change in enthalpy ($\Delta_r H^o$) and entropy ($\Delta_r S^o$) upon adsorption as

https://doi.org/10.1021/acsomega.4c05044
ACS Omega 2024, 9, 38054−38065

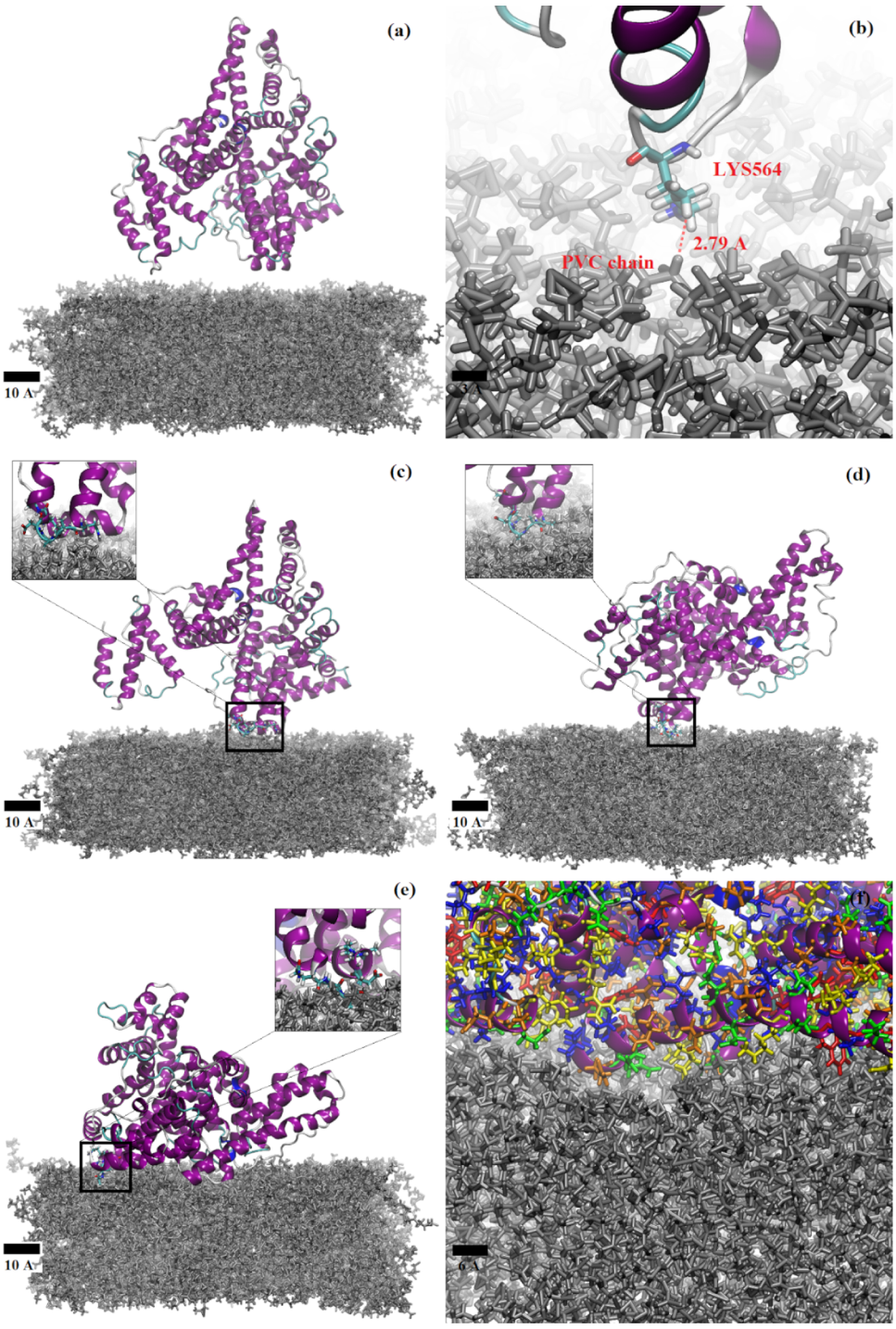

Figure 2. Representative snapshots of the HSA-PVC MD simulation. (a) starting frame; (b) 60 ps: the first contact; (c) 3 ns: interactions of key residues (Gln170, Ala171, Ala172, Asp173, and Lys175) with PVC chains; (d) 150 ns: bending of HSA onto PVC surface; (e) 300 ns: key residues are still in contact with PVC surface while HSA is continuously bending; and (f) 500 ns: different types of amino acid residues interacting with PVC chains (aliphatic, aromatic, polar uncharged, acidic and basic amino acid residues are represented by blue, red, orange, yellow, and green licorice, respectively).

$$\left(\frac{\partial\left(\frac{\Delta_r G^\circ}{T}\right)}{\partial T}\right)_P = -\frac{\Delta_r H^\circ}{T^2} \quad (1)$$

$$\left(\frac{\partial \Delta_r G^\circ}{\partial T}\right)_P = -\Delta_r S^\circ \quad (2)$$

3. RESULTS AND DISCUSSION

3.1. Docking Structure Evaluation. Triplicate docking calculations were conducted for each protein, considering 20 models (poses) of the protein-PVC complex in each calculation. Based on the top-ranked poses obtained from the docking calculations, we identified the amino acids to which the PVC chain preferentially binds and the types of interactions taking place. Figure 1 presents the 2D image and

https://doi.org/10.1021/acsomega.4c05044
ACS Omega 2024, 9, 38054−38065

3D image showing molecular interactions between the PVC chain and HSA protein. Similar representations for FB, C3b, and HTR proteins are shown in Figure S2. The results revealed that hydrophobic interactions play a dominant role in the stability of PVC-protein complexes, aligning with previous results from protein adsorption studies on other inert polymeric materials such as Polystyrene.[39]

The molecular docking results indicate a strong interaction between the PVC chain and HSA protein, with an average binding energy of -25.9 ± 1.2 kJ mol^{-1}. The other three proteins, HTR, C3b, and FB, also exhibit interactions with the PVC chain, with average binding energies of -20.5 ± 1.05, -19.7 ± 0.98, and -14.2 ± 0.55 kJ mol^{-1}, respectively. This behavior mirrors findings in the interaction of HSA, FB, and HTR with polyacrylonitrile hemodialysis clinical membranes, which have binding energies of −29.7, −23.4, and −25.9 kJ mol^{-1}, respectively.[20]

The observation that HSA demonstrates the highest interaction energy among the studied proteins, coupled with its status as the most abundant protein in human plasma (constituting around 60% of the total plasma protein content), underscores its relevance for studying interactions with materials that come into contact with blood. Moreover, HSA is one of the most extensively studied proteins due to its critical physiological functions and therapeutic potential, providing insights into both biocompatibility and toxicity.[63] HSA is known for its ability to bind reversibly or covalently to a wide range of endogenous and exogenous compounds. Unlike other plasma proteins, HSA can bind to a diverse array of ligands and materials with high affinity.[64]

HSA's interaction with numerous polymers, plastics, and microplastics has been extensively investigated.[65−68] This substantial body of research facilitates comparative analysis and provides a contextual framework for our study. The complex binding behavior of HSA is of significant scientific interest. Investigating its interactions with PVC using molecular simulations can enhance our understanding of the molecular mechanisms underlying these interactions, which is crucial for applications in biocompatibility and material science.

3.2. MD Simulations. *3.2.1. Adsorption Mechanism.* The HSA-PVC simulation was performed in triplicates (0.5 μs each) to achieve reliable data for analysis. Figure S3 shows the alignment of the protein structure at the end of the three simulations which indicates the consistency of the results. One of the trajectories was chosen to be studied for the investigation of the adsorption mechanism of HSA onto the PVC surface. The trajectory analysis of the HSA-PVC simulation reveals a dynamic process of adsorption characterized by an initial bending of the HSA protein to maximize surface contact with the PVC substrate. This bending behavior is consistent with the adaptation of the protein structure to achieve optimal interactions with the PVC surface.

As it is shown in Figure 2a, the simulation commenced with the protein in a perpendicular orientation to the PVC layer, reflecting the configuration with the highest docking score from prior docking calculations. With acknowledging that a 2D PVC surface may induce different conformational changes and interaction strengths in HSA, the docking results offer a valuable starting point indicative of potential binding hotspots. Additionally, the long MD simulations (triplicate 0.5 μs trajectories) allowed the protein to relax and adopt conformations driven by the interaction potential with the PVC surface. The approximation from a single PVC chain to a 2D PVC surface is based on the hypothesis that the interaction energy trends observed with a monomer can be extended to a surface. This hypothesis is supported by the literature[45−47] and provides a practical approach given the current computational resources.

In this configuration, the initial contact between HSA and PVC, occurring within the first 60 ps, was facilitated by the involvement of the Lys564 amino acid residue (Figure 2b). The proximity of Lys564 (2.79 Å) indicated a robust hydrophobic interaction, underscoring the significance of such interactions in initiating the adsorption process. Nevertheless, this interaction was transient as the protein dynamically adjusted its configuration to enhance contact with the PVC surface.

A critical phase in the adsorption process unfolded around 3 ns into the simulation, marked by the discernible bending of HSA over the PVC surface. Notably, specific amino acid residues emerged as key players in stabilizing the protein near the PVC surface during its movement, with Gln170, Ala171, Ala172, Asp173, and Lys175 identified as pivotal residues (Figure 2c). These residues displayed recurrent interactions with various PVC chains, signifying their importance in mediating and stabilizing the adsorption of HSA onto the PVC surface (Figure 2d,e).

Further characterization of the interactions revealed a diversity of amino acid types involved, including aliphatic, aromatic, polar uncharged, acidic, and basic amino acids. This diversity underscores the complex nature of the HSA-PVC interaction, with different amino acid residues contributing to the stability of the adsorbed state. Figure 2f provides a visual representation of the equilibrium phase, illustrating the distribution and nature of amino acid residues in contact with the PVC surface.

The system achieved equilibrium after approximately 350 ns of the simulation time, persisting until the conclusion of the trajectory. The observed equilibrium indicates a stabilized state of HSA adsorption onto PVC, reinforcing the reliability and validity of the simulation results.

To enhance the accuracy of our simulation descriptions, we conducted a comprehensive density profile analysis along the z-axis direction for all components within the systems. Figure S4 illustrates a uniform distribution of water molecules around the protein in the reference simulation, indicating a well-equilibrated environment.

In contrast, Figure 3 portrays the density profile of the HSA-PVC system. This system exhibits a stratified composition with

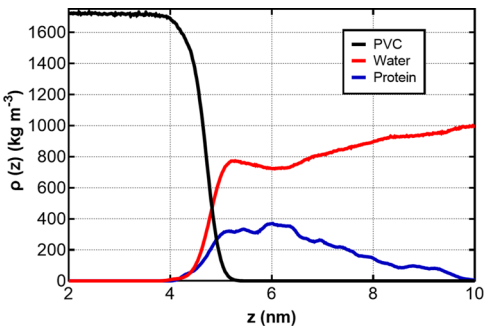

Figure 3. Density profile of the components of the HSA-PVC system at equilibrium.

https://doi.org/10.1021/acsomega.4c05044
ACS Omega 2024, 9, 38054−38065

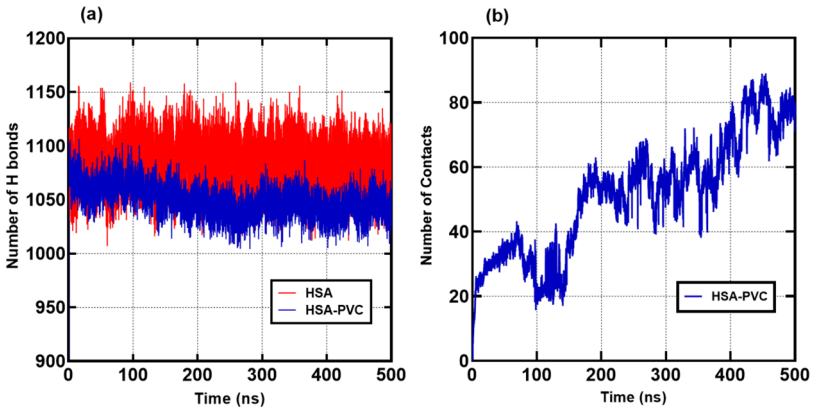

Figure 4. (a) Total number of hydrogen bonds between HSA and water as a function of time; (b) Total number of HSA protein residues in contact with PVC surface as a function of time.

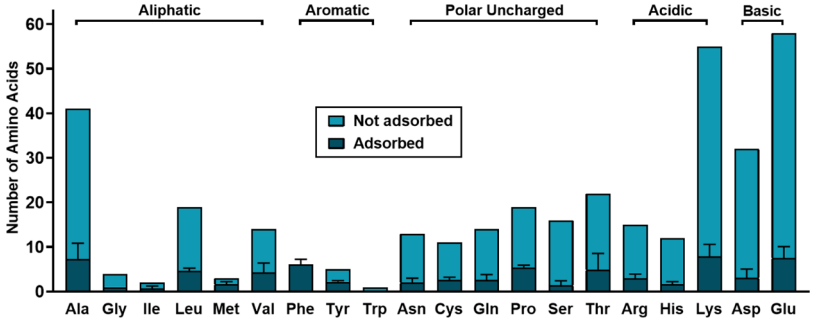

Figure 5. Number of HSA amino acids (three-letter code) adsorbed (in contact with PVC surface) and not absorbed (surface residues not in contact with PVC surface) at equilibrium.

distinct regions along the *z*-axis. At the bottom, there is a PVC slab, forming the substrate. Above it, an interface layer emerges, comprising the protein and some water molecules. This interfacial region extends over about 15 Å. From this distance, the water molecules recover their bulk properties. The remaining protein and water molecules occupy the uppermost region. This observation signifies a multilayered arrangement, emphasizing the distinct spatial organization of the protein and water within the HSA-PVC system.

Comparative analysis of the density profiles between the reference and HSA-PVC systems reveals the strategic positioning of the protein within the latter. The proximity of the protein to the PVC surface is evident, confirming the reliability of the simulation setup in mimicking the adsorption scenario. Moreover, the observed distribution of water molecules further highlights the importance of the hydration layer in facilitating and modulating protein−polymer interactions.

In our quest to unravel the intricacies of HSA adsorption onto PVC, we commenced by scrutinizing the interactions between HSA and water molecules. Figure 4a illustrates that the introduction of the PVC surface led to a reduction in the total number of hydrogen bonds formed between HSA and water. This reduction indicates a dynamic shift in the protein's interaction preferences in the presence of the PVC substrate.

To gain a more comprehensive understanding of the evolving interactions, we turned our attention to the total number of contacts established between HSA and the PVC surface by considering that the surface is in contact with one amino acid if they have at least one pair of atoms separated by a distance not larger than 3.5 Å.[39,40] Figure 4b unveils the increase in contacts between HSA and PVC with time.

The substantial decrease in hydrogen bonds with water coincides with a corresponding rise in contacts with the PVC surface. This observation aligns with the notion that the availability of the PVC surface influenced the interaction preferences of HSA, leading to a shift from water-mediated interactions to direct interactions with the polymer. These findings underscore the dynamic nature of the adsorption process, shedding light on the interplay between HSA, water, and the PVC surface.

A further breakdown of the number of contacts made by individual amino acid types was performed to elucidate the specific residues responsible for the interactions. Figure 5 provides an insightful comparison, showcasing the number of residues in contact with the PVC surface for each amino acid type against the available surface residues not interacting with PVC. The total number of surface residues of HSA was computed using the Swiss-PdbViewer software V.4.1[69] with a 10% cutoff value, meaning that a residue is considered a surface residue if at least 10% of this residue is surface-accessible.

The results depicted in Figure 5 underscore the diverse nature of interactions between HSA and PVC, spanning across various types of amino acid groups. This diversity is expected given the substantial size of HSA (comprising 578 amino acid residues, of which 362 residues are surface-accessible), the heterogeneous nature of residues, and the chemical characteristics of PVC.

To offer a more granular perspective on these interactions, Table 1 presents the percentage of each amino acid group and their respective adsorption on the PVC surface. This detailed breakdown highlights the differential contribution of amino acid types to the overall adsorption phenomenon and the

https://doi.org/10.1021/acsomega.4c05044
ACS Omega 2024, 9, 38054−38065

Table 1. Percentage of Each Group of Amino Acids of HSA Adsorbed onto the PVC Surface at Equilibrium

	adsorbed	not adsorbed	surface residues	percentage adsorbed
aliphatic	19 ± 2	64 ± 2	83	22.9 ± 2.8
aromatic	8 ± 1	4 ± 1	12	68.9 ± 8.0
polar uncharged	20 ± 3	75 ± 3	95	21.1 ± 3.4
acidic	13 ± 3	69 ± 3	82	15.3 ± 3.8
basic	11 ± 4	79 ± 4	90	11.8 ± 4.9

significance of the presence of hydrophobic AAs on the protein surface.

In summary, the analysis reveals that HSA utilizes a spectrum of diverse interactions with the PVC surface, notably hydrophobic interactions with hydrophobic AAs; leading to the establishment of a highly stable equilibrium state. This finding raises concerns about the potential high affinity of HSA for adsorption, which could have implications for biofouling processes. The ability of HSA to form varied interactions proves its versatility in mediating interactions with surfaces, a factor that warrants careful consideration in applications involving biomaterial interfaces.

To gain a more quantitative understanding of HSA-PVC interactions, we conducted analyses of the contact area and the Lennard-Jones (LJ) interaction energy profiles.

The contact area was derived using the calculation of the solvent-accessible surface area (SASA) for the protein (HSA) alone, the polymer (PVC) alone, and the HSA-PVC complex:[70]

$$\text{contact area} = \frac{1}{2} \times (\text{SASA}_{\text{HSA}} + \text{SASA}_{\text{PVC}} - \text{SASA}_{\text{HSA-PVC complex}}) \quad (3)$$

As illustrated in Figure 6, the contact area between HSA and the PVC surface exhibited an interesting temporal evolution.

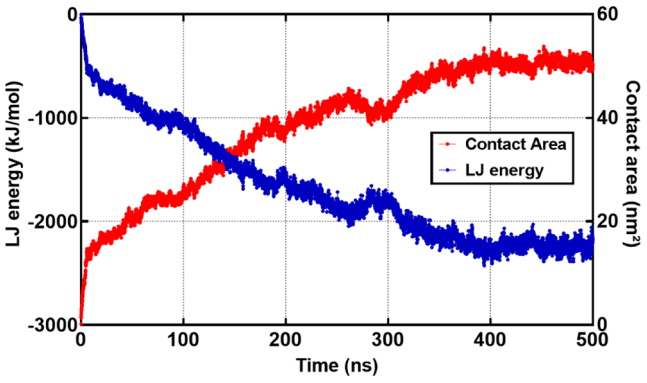

Figure 6. Contact area and LJ interaction energy profile for HSA protein and PVC surface as a function of time.

Initially, it showed a positive value within the first nanoseconds, surpassing the assigned 5 Å gap distance in our system. This phase corresponds to the initial interaction between HSA and PVC, indicating the overcoming of the initial gap distance. Subsequently, a notable gradual increase in the contact area was observed for approximately 350 ns. The system reached an equilibrium stage around the time 350 ns and remained stable until the end of the simulation.

The LJ interaction energy profile, generated using GROMACS, provided additional insights into the dynamic nature of HSA-PVC interactions. As depicted in Figure 6, the LJ energy trend paralleled the calculations of the contact area. At the onset of the simulation, a rapid decrease in LJ energy was observed, reaching approximately −500 kJ mol^{-1}. Subsequently, the LJ energy gradually decreased indicating the evolving and strengthening interactions. Finally, during the equilibrium phase, the LJ energy values continued to decrease, reaching approximately −2200 kJ mol^{-1}, suggesting a stable and energetically favorable state of HSA adsorption onto the PVC surface.

This congruence between the contact area and LJ energy trends reinforces the reliability of our quantitative analyses and provides a comprehensive perspective on the evolving HSA-PVC interactions.

3.2.2. Adsorption Thermodynamics: PMF Calculations. To delve into the adsorption behavior and binding strength of HSA onto the PVC surface, we conducted PMF calculations. These calculations, though extensive and time-consuming, are essential for unraveling the driving forces involved in the adsorption of HSA. The final MD simulation configuration was selected as the initial configuration for meaningful insights. The resulting PMF profiles at different temperatures, as depicted in Figure 7a, indicate the thermodynamically favorable process of HSA adsorption onto PVC. The well-defined curves with significantly negative values (Figure 7a) highlight that the adsorption process is thermodynamically favored.

Notably, the minimum values of the free energy of adsorption were −535 kJ mol^{-1} at 290 K, −507 kJ mol^{-1} at 300 K, and −459 kJ mol^{-1} at 310 K, highlighting the presence of robust interactions between HSA and the PVC surface. These values align with findings from other studies, which report high Gibbs free energy values for protein adsorption on polymer surfaces. For example, the free energy values for the adsorption of cardiotoxin (CTX) protein on mixed self-assembled monolayer (SAM) surfaces can reach up to −300 kJ mol^{-1}.[71]

To dissect the components of the Gibbs free energy profile, we examined the variation of free energy against temperature (Figure 7b). The derived values indicate that the adsorption process of HSA onto the PVC surface is spontaneous, and primarily driven by enthalpy ($\Delta_r H^\circ$ = −1647 kJ mol^{-1}). The negative entropy change ($T\Delta_r S^\circ$ = −1140 kJ mol^{-1}) clearly establishes the loss of degrees of freedom of HSA upon adsorption. In addition, the strong LJ interactions between HSA protein and PVC surface is in line with an adsorption process governed by the enthalpy.

Further exploration into the enthalpy and entropy changes along the reaction coordinate revealed consistent trends, aligning with the negative values of $\Delta_r G^\circ$ at various temperatures (Figure S5). This reinforces the enthalpy-driven and spontaneous nature of the adsorption process.

The signs and values of $\Delta_r H^\circ$ and $\Delta_r S^\circ$ were utilized to identify the key interaction forces driving the adsorption reactions.[72] With both $\Delta_r H^\circ$ and $\Delta_r S^\circ$ being negative, we can infer that van der Waals forces and hydrogen bonds played predominant roles in the adsorption process. This finding is consistent with some interactions involving key residues. While direct hydrogen bonds between HSA and the PVC surface were not identified, water-mediated hydrogen bonds formed in

https://doi.org/10.1021/acsomega.4c05044
ACS Omega 2024, 9, 38054−38065

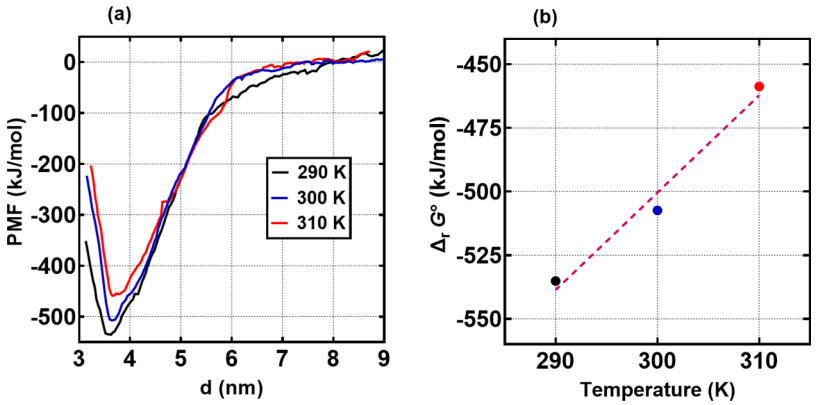

Figure 7. (a) PMF profiles calculated at different temperatures as a function of the distance between the center of mass of HSA and the center of mass of PVC along their reaction coordinate; (b) The variation of Gibbs free energy calculated at different temperatures during the adsorption process of HSA onto PVC surface as a function of temperature; yielding the equation of the line ($y = 3.822x - 1647$).

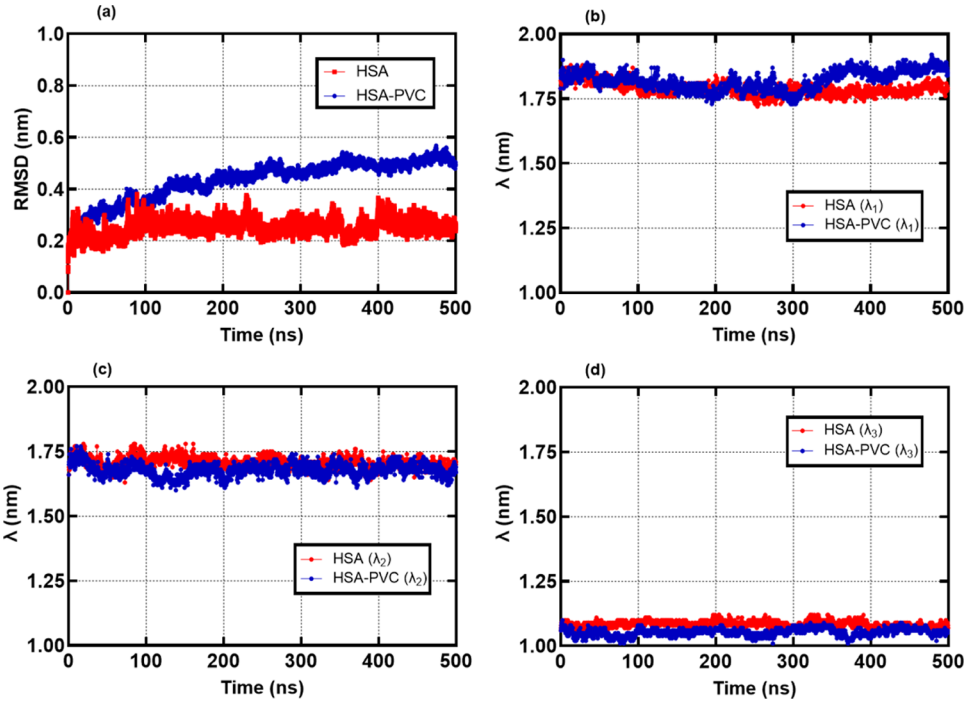

Figure 8. (a) Root-mean-square deviation (RMSD) of all backbone carbon atoms of HSA protein and (b–d) the eigenvalues of Rg for HSA protein during the 0.5 μs MD simulations.

the presence of water molecules at the interface layer facilitated interactions between HSA and PVC chains (Figure S6).

3.2.3. Conformational and Structural Changes of HSA. To investigate the conformational and potential structural alterations of HSA during the simulations, we conducted a series of analyses comparing the HSA-PVC simulation with our reference simulation.

3.2.3.1. Root-Mean-Square Deviation (RMSD). The RMSD of the backbone atoms of HSA relative to the crystal structure was calculated to assess the overall stability of the protein structure. As depicted in Figure 8a, the RMSD in the HSA-PVC simulation indicated the stability of the system but with a slight increase compared to the reference simulation. However, this difference, not exceeding 3 Å at equilibrium, suggests necessary minor conformational changes facilitating the complete adsorption of HSA onto the PVC surface.

3.2.3.2. Radius of Gyration (R_g). The eigenvalues of R_g were calculated to gauge the compactness and folding state of the protein. Figure 8b–d indicates that the change in R_g was primarily driven by alterations in the x-axis component of the eigenvalues ($\lambda 1$) starting around 350 ns until the end of the simulation. This points to a localized change in a specific region of HSA that interacts with the PVC surface, while the overall structure remained globally stable.

To corroborate this observation, the total R_g was calculated, revealing relatively stable values during both simulations (Figure S7; the mean values of 2.68 ± 0.02 and 2.73 ± 0.03 nm for HSA in the reference simulation and in the HSA-PVC simulation, respectively.). In addition, the R_g density distribution is represented in Figure S8; showing a small shift in the population of R_g values between the HSA-PVC simulation and the reference simulation. Hence, the minor

https://doi.org/10.1021/acsomega.4c05044
ACS Omega 2024, 9, 38054–38065

increase observed in the HSA-PVC system corresponds to the change in the x-axis component of the eigenvalues.

3.2.3.3. Volume and Solvent-Accessible Surface Area (SASA). Additional analyses on the protein volume and its solvent-accessible surface area (SASA) showed constant values throughout the simulations (Figure S9a,b). No significant differences were observed between the reference simulation and the HSA-PVC simulation, suggesting that the overall protein structure remained unaffected by the adsorption process.

3.2.3.4. Secondary Structure Analysis. The secondary structure analysis using the DSSP module of GROMACS demonstrated that the secondary structure features of HSA did not undergo significant changes upon adsorption onto the PVC slab (Table 2). The calculated abundance of the α-helical conformation is consistent with previously reported values.[73,74] The obtained values indicate that the adsorption process did not induce major alterations in the secondary structure of HSA. Figure S10 represents the alignment of the protein structure before and after adsorption on PVC surface confirming no substantial structural change. These findings are consistent with experimental Circular Dichroism (CD) results, which indicate that the secondary structure of HSA remains stable and shows little to no significant change upon binding to different polymeric materials such as polyoxometalates (POMs).[75]

Table 2. Percentage of Secondary Structures of HSA in the MD simulations

	coil	bend	turn	α-helix
HSA	14.0 ± 0.5	7.1 ± 0.7	7.3 ± 1.3	68.9 ± 1.2
HSA-PVC	14.0 ± 0.6	7.4 ± 0.8	8.0 ± 1.1	69.0 ± 1.2

Collectively, the analyses suggest that the interaction with the PVC surface induced localized changes in HSA's conformation and tertiary structures, facilitating increased accessibility of amino acid residues at the polymer surface. However, it is crucial to note that stability in secondary and tertiary structures does not guarantee the proper functioning of HSA after adsorption onto PVC. Furthermore, the formation of an attractive layer for other cells on the HSA molecules may initiate the biofouling process, a concern particularly relevant in medical devices employing PVC surfaces extensively.

4. CONCLUSIONS

The biofouling phenomenon plays a pivotal role in defining the biocompatibility of medical devices, with the adsorption affinity of plasma proteins on biomaterial surfaces serving as a critical determinant. In this study, we employed computational techniques to unravel the molecular-level interactions governing protein adsorption onto PVC. Through extensive analyses, we identified HSA as the most relevant plasma protein for studying its adsorption onto PVC.

MD simulations were conducted for HSA in water (as a reference simulation) and HSA on the PVC surface. Five key residues (Gln170, Ala171, Ala172, Asp173, and Lys175) were pinpointed as crucial for the adsorption mechanism. Various analyses, including contact calculations, contact area determination, and interaction energy assessments, provided consistent and comprehensive insights into the interactions between HSA and the PVC surface.

Thermodynamic aspects of the adsorption process were evaluated through extensive PMF calculations at different temperatures. The Gibbs free energy of adsorption indicated strong interactions between HSA and PVC surface, with values of −535 kJ mol^{-1} (290 K), −507 kJ mol^{-1} (300 K), and −458 kJ mol^{-1} (310 K). The adsorption process was found to be spontaneous, thermodynamically favored, and primarily driven by enthalpy ($\Delta_r H^\circ$ = −1647 kJ mol^{-1}), with water-mediated hydrogen bonds and van der Waals forces identified as key contributors.

Structural analyses demonstrated that the global structure of HSA remained stable, with localized changes facilitating increased accessibility of amino acid residues at the polymer surface. This study offers a comprehensive evaluation of a crucial process influencing the biocompatibility of medical devices at the molecular level. The insights gained can inform the design of PVC surfaces tailored for specific biomolecular interactions, with broad applications in materials science, biotechnology, and biomedical engineering.

Potential new investigations would concern the interactions with other plasma proteins and diverse biomaterials and the challenging aspect of multimolecular cooperativity between adsorbed proteins on a single polymeric surface. These simulations potential will help to improve our understanding of the biofouling process and of the biocompatibility of medical devices.

■ ASSOCIATED CONTENT

Supporting Information

The Supporting Information is available free of charge at https://pubs.acs.org/doi/10.1021/acsomega.4c05044.

MD simulation systems' composition, docking images, triplicate simulations HSA structure alignment, density profile, enthalpy and entropy profiles, water-mediated H-bond, R_g total, R_g density distribution, volume and SASA, initial and final HSA structure alignment (PDF)

■ AUTHOR INFORMATION

Corresponding Authors

Patrice Malfreyt − *Université Clermont Auvergne, CNRS, Clermont Auvergne INP, Institut de Chimie de Clermont-Ferrand, F-63000 Clermont-Ferrand, France;* orcid.org/0000-0002-3710-5418; Email: patrice.malfreyt@uca.fr

Mehdi Sahihi − *Université Clermont Auvergne, CNRS, Clermont Auvergne INP, Institut de Chimie de Clermont-Ferrand, F-63000 Clermont-Ferrand, France;* orcid.org/0000-0003-2923-1833; Email: mehdi.sahihi@uca.fr

Authors

Amr H. Saleh − *Université Clermont Auvergne, CNRS, Clermont Auvergne INP, Institut de Chimie de Clermont-Ferrand, F-63000 Clermont-Ferrand, France;* orcid.org/0000-0002-3175-1048

Ghazal Borhan − *Université Clermont Auvergne, CNRS, Clermont Auvergne INP, Institut de Chimie de Clermont-Ferrand, F-63000 Clermont-Ferrand, France*

Florent Goujon − *Université Clermont Auvergne, CNRS, Clermont Auvergne INP, Institut de Chimie de Clermont-Ferrand, F-63000 Clermont-Ferrand, France;* orcid.org/0000-0001-7511-3905

https://doi.org/10.1021/acsomega.4c05044
ACS Omega 2024, 9, 38054−38065

Julien Devémy − *Université Clermont Auvergne, CNRS, Clermont Auvergne INP, Institut de Chimie de Clermont-Ferrand, F-63000 Clermont-Ferrand, France*

Alain Dequidt − *Université Clermont Auvergne, CNRS, Clermont Auvergne INP, Institut de Chimie de Clermont-Ferrand, F-63000 Clermont-Ferrand, France;* orcid.org/0000-0003-1206-1911

Complete contact information is available at: https://pubs.acs.org/10.1021/acsomega.4c05044

Notes

The authors declare no competing financial interest.

■ ACKNOWLEDGMENTS

This work was performed in SimatLab, a joint public-private laboratory dedicated to the modeling of polymer materials. This laboratory is supported by Michelin, Clermont Auvergne University (UCA), CHU Clermont-Ferrand and CNRS. We are grateful to the Mésocentre Clermont Auvergne University for providing computing and storage resources.

■ REFERENCES

(1) Vroman, L.; Adams, A. L. Effect of heparin on reactions at aminated polymer—blood interfaces. *J. Colloid Interface Sci.* **1969**, *31*, 188−195.

(2) Brash, J. L.; Ten Hove, P. Transient adsorption of fibrinogen on foreign surfaces: similar behavior in plasma and whole blood. *J. Biomed. Mater. Res.* **1989**, *23*, 157−169.

(3) Banerjee, I.; Pangule, R. C.; Kane, R. S. Antifouling Coatings: Recent Developments in the Design of Surfaces That Prevent Fouling by Proteins, Bacteria, and Marine Organisms. *J. Adv. Mater.* **2011**, *23*, 690−718.

(4) Nakanishi, K.; Sakiyama, T.; Imamura, K. On the adsorption of proteins on solid surfaces, a common but very complicated phenomenon. *J. Biosci. Bioeng.* **2001**, *91*, 233−244.

(5) Harding, J. L.; Reynolds, M. M. Combating medical device fouling. *Trends Biotechnol.* **2014**, *32*, 140−146.

(6) O'Toole, G. A. A resistance switch. *Nature* **2002**, *416*, 695−696.

(7) Vadgama, P. 2 Surface biocompatibility. *Annu. Rep. Prog. Chem., Sect. C* **2005**, *101*, 14−52.

(8) Bullock, C. J.; Bussy, C. Biocompatibility considerations in the design of graphene biomedical materials. *Adv. Mater. Interfaces* **2019**, *6*, No. 1900229.

(9) Williams, D. F. Biocompatibility pathways and mechanisms for bioactive materials: The bioactivity zone. *Bioact. Mater.* **2022**, *10*, 306−322.

(10) Gamucci, O.; Bertero, A.; Gagliardi, M.; Bardi, G. Biomedical nanoparticles: overview of their surface immune-compatibility. *Coatings* **2014**, *4*, 139−159.

(11) Brash, J. L.; Horbett, T. A.; Latour, R. A.; Tengvall, P. The blood compatibility challenge. Part 2: Protein adsorption phenomena governing blood reactivity. *Acta Biomater.* **2019**, *94*, 11−24.

(12) Chen, K.; Ustriyana, P.; Moore, F.; Sahai, N. Biological response of and blood plasma protein adsorption on silver-doped hydroxyapatite. *ACS Biomater. Sci. Eng.* **2019**, *5*, 561−571.

(13) Geyer, R.; Jambeck, J. R.; Law, K. L. Production, use, and fate of all plastics ever made. *Sci. Adv.* **2017**, *3*, No. e1700782.

(14) ltd, R. *Markets Polyvinyl chloride (PVC) market - growth, trends, COVID-19 impact, and forecasts (2023−2028)*, 2023.

(15) Czogała, J.; Pankalla, E.; Turczyn, R. Recent Attempts in the Design of Efficient PVC Plasticizers with Reduced Migration. *Materials* **2021**, *14*, 844.

(16) Festas, A.; Ramos, A.; Davim, J. Medical devices biomaterials−A review. *Proc. Inst. Mech. Eng., Part L* **2020**, *234*, 218−228.

(17) Domonkos, C.; Zsila, F.; Fitos, I.; Visy, J.; Kassai, R.; Bálint, B.; Kotschy, A. Synthesis and serum protein binding of novel ring-substituted harmine derivatives. *RSC Adv.* **2015**, *5*, 53809−53818.

(18) Sahihi, M.; Borhan, G. The effects of single-walled carbon nanotubes (SWCNTs) on the structure and function of human serum albumin (HSA): Molecular docking and molecular dynamics simulation studies. *J. Struct. Chem.* **2017**, *28*, 1815−1822.

(19) Nonckreman, C. J.; Fleith, S.; Rouxhet, P. G.; Dupont-Gillain, C. C. Competitive adsorption of fibrinogen and albumin and blood platelet adhesion on surfaces modified with nanoparticles and/or PEO. *Colloids Surf., B* **2010**, *77*, 139−149.

(20) Saadati, S.; Eduok, U.; Westphalen, H.; Abdelrasoul, A.; Shoker, A.; Choi, P.; Doan, H.; Ein-Mozaffari, F.; Zhu, N. Assessment of polyethersulfone and polyacrylonitrile hemodialysis clinical membranes: In situ synchrotron-based imaging of human serum proteins adsorption, interaction analyses, molecular docking and clinical inflammatory biomarkers investigations. *Mater. Today Commun.* **2021**, *29*, No. 102928.

(21) Güette-Fernández, J. R.; Meléndez, E.; Maldonado-Rojas, W.; Ortega-Zúñiga, C.; Olivero-Verbel, J.; Parés-Matos, E. I. A molecular docking study of the interactions between human transferrin and seven metallocene dichlorides. *J. Mol. Graphics Modell.* **2017**, *75*, 250−265.

(22) Avidan, O.; Satanower, S.; Banin, E. Iron and bacterial biofilm development. *Microbial Mats* **2010**, *14*, 359−383.

(23) Biryukov, S.; Stoute, J. A.The complement system. In *Complement Activation in Malaria Immunity and Pathogenesis* 2018; pp 1−29 .

(24) Kizhakkedathu, J. N.; Conway, E. M. Biomaterial and cellular implants: foreign surfaces where immunity and coagulation meet. *Blood* **2022**, *139*, 1987−1998.

(25) Ding, T.; Sun, J. Formation of protein corona on nanoparticle affects different complement activation pathways mediated by C1q. *Pharm. Res.* **2020**, *37*, No. 10.

(26) Gizer, G.; Önal, U.; Ram, M.; Şahiner, N. Biofouling and mitigation methods: A review. *Biointerface Res. Appl. Chem.* **2023**, *13* (2), No. 185, DOI: 10.33263/briac132.185.

(27) Nagase, K.; Onuma, T.; Yamato, M.; Takeda, N.; Okano, T. Enhanced Wettability Changes by Synergistic Effect of Micro/Nanoimprinted Substrates and Grafted Thermoresponsive Polymer Brushes. *Macromol. Rapid Commun.* **2015**, *36*, 1965−1970.

(28) Koguchi, R.; Jankova, K.; Tanaka, Y.; Yamamoto, A.; Murakami, D.; Yang, Q.; Ameduri, B.; Tanaka, M. Altering the bio-inert properties of surfaces by fluorinated copolymers of mPEGMA. *Biomater. Adv.* **2023**, *153*, No. 213573.

(29) Ray, S.; Shard, A. G. Quantitative analysis of adsorbed proteins by X-ray photoelectron spectroscopy. *Anal. Chem.* **2011**, *83*, 8659−8666.

(30) Hedberg, Y. S.; Killian, M. S.; Blomberg, E.; Virtanen, S.; Schmuki, P.; Odnevall Wallinder, I. Interaction of bovine serum albumin and lysozyme with stainless steel studied by time-of-flight secondary ion mass spectrometry and X-ray photoelectron spectroscopy. *Langmuir* **2012**, *28*, 16306−16317.

(31) Heesink, G.; Marseille, M. J.; Fakhree, M. A. A.; Driver, M. D.; van Leijenhorst-Groener, K. A.; Onck, P. R.; Blum, C.; Claessens, M. M. Exploring Intra- and Inter-Regional Interactions in the IDP a-Synuclein Using smFRET and MD Simulations. *Biomacromolecules* **2023**, *24*, 3680−3688.

(32) Jahan Sajib, M. S.; Wei, Y.; Mishra, A.; Zhang, L.; Nomura, K.-I.; Kalia, R. K.; Vashishta, P.; Nakano, A.; Murad, S.; Wei, T. Atomistic Simulations of Biofouling and Molecular Transfer of a Cross-linked Aromatic Polyamide Membrane for Desalination. *Langmuir* **2020**, *36*, 7658−7668.

(33) AlRawashdeh, S.; Barakat, K. H. *Computational Drug Discovery and Design*; Springer, 2023; pp 127−141.

(34) Yagasaki, T.; Matubayasi, N. Molecular dynamics study of the interactions between a hydrophilic polymer brush on graphene and amino acid side chain analogues in water. *Phys. Chem. Chem. Phys.* **2022**, *24*, 22877−22888.

(35) Yasoshima, N.; Ishiyama, T.; Matubayasi, N. Adsorption Energetics of Amino Acid Analogs on Polymer/Water Interfaces Studied by All-Atom Molecular Dynamics Simulation and a Theory of Solutions. *J. Phys. Chem. B* **2022**, *126*, 4389−4400, DOI: 10.1021/acs.jpcb.2c01297.
(36) Feng, J.; Slocik, J. M.; Sarikaya, M.; Naik, R. R.; Farmer, B. L.; Heinz, H. Influence of the Shape of Nanostructured Metal Surfaces on Adsorption of Single Peptide Molecules in Aqueous Solution. *Small* **2012**, *8*, 1049−1059.
(37) Zhao, D.; Peng, C.; Zhou, J. Lipase adsorption on different nanomaterials: a multi-scale simulation study. *Phys. Chem. Chem. Phys.* **2015**, *17*, 840−850.
(38) Pfaff, L.; Gao, J.; Li, Z.; Jäckering, A.; Weber, G.; Mican, J.; Chen, Y.; Dong, W.; Han, X.; Feiler, C. G.; Ao, Y. F.; znd Christoffel PS Badenhorst, Y.-F. A.; Badenhorst, C. P. S.; Bednar, D.; Bednar, D.; Palm, G. J.; Palm, G. J.; Lammers, M.; Lammers, M.; Damborsky, J.; Damborsky, J.; Strodel, B.; Strodel, B.; Liu, W.; Liu, W.; Bornscheuer, U. T.; Bornscheuer, U. T.; Wei, R. Multiple Substrate Binding Mode-Guided Engineering of a Thermophilic PET Hydrolase. *ACS Catal.* **2022**, *12*, 9790−9800.
(39) Sahihi, M.; Faraudo, J. Molecular Dynamics Simulations of Adsorption of SARS-CoV-2 Spike Protein on Polystyrene Surface. *J. Chem. Inf. Model.* **2022**, *62*, 3814−3824.
(40) Sahihi, M.; Faraudo, J. Computer Simulation of the interaction between SARS-CoV-2 Spike Protein and the Surface of Coinage Metals. *Langmuir* **2022**, *38*, 14673−14685.
(41) Tokhadzé, N.; Sahnoune, M.; Devémy, J.; Dequidt, A.; Goujon, F.; Chennell, P.; Sautou, V.; Malfreyt, P. Insulin Adsorption Onto PE and PVC Tubings. *ACS Appl. Bio Mater.* **2022**, *5*, 2567−2575.
(42) Tang, Y. Z.; Chen, W. Z.; Wang, C. X.; Shi, Y. Y. Constructing the suitable initial configuration of the membrane-protein system in molecular dynamics simulations. *Eur. Biophys. J.* **1999**, *28*, 478−488.
(43) Sishi, Z.; Bahig, J.; Kalugin, D.; Shoker, A.; Zhu, N.; Abdelrasoul, A. Influence of clinical hemodialysis membrane morphology and chemistry on protein adsorption and inflammatory biomarkers released: In-situ synchrotron imaging, clinical and computational studies. *Biomed. Eng. Adv.* **2023**, *5*, No. 100070.
(44) Saadati, S.; Eduok, U.; Westphalen, H.; Abdelrasoul, A.; Shoker, A.; Choi, P.; Doan, H.; Ein-Mozaffari, F.; Zhu, N. In situ synchrotron imaging of human serum proteins interactions, molecular docking and inflammatory biomarkers of hemocompatible synthesized zwitterionic polymer coated-polyvinylidene fluoride (PVDF) dialysis membranes. *Surf. Interfaces* **2021**, *27*, No. 101505.
(45) Saadati, S.; Westphalen, H.; Eduok, U.; Abdelrasoul, A.; Shoker, A.; Choi, P.; Doan, H.; Ein-Mozaffari, F.; Zhu, N. Biocompatibility enhancement of hemodialysis membranes using a novel zwitterionic copolymer: Experimental, in situ synchrotron imaging, molecular docking, and clinical inflammatory biomarkers investigations. *Mater. Sci. Eng.: C* **2020**, *117*, 111301.
(46) Boroznjak, R.; Reut, J.; Tretjakov, A.; Lomaka, A.; Öpik, A.; Syritski, V. A computational approach to study functional monomer-protein molecular interactions to optimize protein molecular imprinting. *J. Mol. Recognit.* **2017**, *30*, e2635.
(47) Li, J.; Feng, J.; Dang, Q.; Qiao, Y.; Zhao, J.; Zhang, S.; Sun, H.; Wen, X.; Yuan, Z. Affinity adsorption mechanism studies of adsorbents for oligopeptides using model polymer. *Polymer* **2009**, *50*, 1602−1608.
(48) Dennington, R.; Keith, T. A.; Millam, J. M. *GaussView Version 6*; Semichem Inc.: Shawnee Mission KS, 2019.
(49) Frisch, M. J.; Trucks, G. W.; Schlegel, H. B.; Scuseria, G. E.; Robb, M. A.; Cheeseman, J. R.; Scalmani, G.; Barone, V.; Petersson, G. A.; Nakatsuji, H.; Li, X.; Caricato, M.; Marenich, A. V.; Bloino, J.; Janesko, B. G.; Gomperts, R.; Mennucci, B.; Hratchian, H. P.; Ortiz, J. V.; Izmaylov, A. F.; Sonnenberg, J. L.; Williams-Young, D.; Ding, F.; Lipparini, F.; Egidi, F.; Goings, J.; Peng, B.; Petrone, A.; Henderson, T.; Ranasinghe, D.; Zakrzewski, V. G.; Gao, J.; Rega, N.; Zheng, G.; Liang, W.; Hada, M.; Ehara, M.; Toyota, K.; Fukuda, R.; Hasegawa, J.; Ishida, M.; Nakajima, T.; Honda, Y.; Kitao, O.; Nakai, H.; Vreven, T.; Throssell, K.; Montgomery, J. A., Jr.; Peralta, J. E.; Ogliaro, F.; Bearpark, M. J.; Heyd, J. J.; Brothers, E. N.; Kudin, K. N.; Staroverov, V. N.; Keith, T. A.; Kobayashi, R.; Normand, J.; Raghavachari, K.; Rendell, A. P.; Burant, J. C.; Iyengar, S. S.; Tomasi, J.; Cossi, M.; Millam, J. M.; Klene, M.; Adamo, C.; Cammi, R.; Ochterski, J. W.; Martin, R. L.; Morokuma, K.; Farkas, O.; Foresman, J. B.; Fox, D. J. *Gaussian16*, Revision C.01; Gaussian Inc.: Wallingford CT, 2016.
(50) Vriend, G. WHAT IF: a molecular modeling and drug design program. *J. Mol. Graphics* **1990**, *8*, 52−56.
(51) Eberhardt, J.; Santos-Martins, D.; Tillack, A. F.; Forli, S. AutoDock Vina 1.2. 0: New docking methods, expanded force field, and python bindings. *J. Chem. Inf. Model.* **2021**, *61*, 3891−3898.
(52) Trott, O.; Olson, A. J. AutoDock Vina: improving the speed and accuracy of docking with a new scoring function, efficient optimization, and multithreading. *J. Comput. Chem.* **2010**, *31*, 455−461.
(53) Laskowski, R. A.; Swindells, M. B. LigPlot+: multiple ligand-protein interaction diagrams for drug discovery. *J. Chem. Inf. Model.* **2011**, *51* (10), 2778−2786, DOI: 10.1021/ci200227u.
(54) Oh, K. H.; Ko, Y.-H.; Kim, K.-J. Mechanical properties of amorphous PEI, PES, and PVC up to 11 GPa studied by Brillouin light scattering. *Phys. B: Condens.* **2020**, *576*, No. 411722.
(55) Tokhadzé, N.; Sahnoune, M.; Devémy, J.; Dequidt, A.; Goujon, F.; Chennell, P.; Sautou, V.; Malfreyt, P. Insulin adsorption onto PE and PVC tubings. *ACS Appl. Bio Mater.* **2022**, *5*, 2567−2575.
(56) Berendsen, H. J.; van der Spoel, D.; van Drunen, R. GROMACS: A message-passing parallel molecular dynamics implementation. *Comput. Phys. Commun.* **1995**, *91*, 43−56.
(57) Lindahl, E.; Hess, B.; Van Der Spoel, D. GROMACS 3.0: a package for molecular simulation and trajectory analysis. *J. Mol. Model.* **2001**, *7*, 306−317.
(58) Van Der Spoel, D.; Hess, B.; Lindahl, E.; Van Der Spoel, D.; Mark, A.; Groenhof, G. GROMACS: fast, flexible, and free. *J. Comput. Chem.* **2005**, *26*, 1701−1718.
(59) Abraham, M. J.; Murtola, T.; Schulz, R.; Páll, S.; Smith, J. C.; Hess, B.; Lindahl, E. GROMACS: High performance molecular simulations through multi-level parallelism from laptops to supercomputers. *Softwarex* **2015**, *1−2*, 19−25.
(60) Humphrey, W.; Dalke, A.; Schulten, K. VMD − Visual Molecular Dynamics. *J. Mol. Graphics* **1996**, *14*, 33−38.
(61) Hub, J. S.; De Groot, B. L.; van der Spoel, D. g_wham A Free Weighted Histogram Analysis Implementation Including Robust Error and Autocorrelation Estimates. *J. Chem. Theory Comput.* **2010**, *6*, 3713−3720.
(62) Sahihi, M.; Bordbar, A.; Ghayeb, Y. Thermodynamic denaturation of β-lactoglobulin in the presence of cetylpyridinium chloride. *J. Chem. Thermodyn.* **2010**, *42*, 1423−1428.
(63) Tao, H.-y.; Wang, R.-q.; Sheng, W.-j.; Zhen, Y.-s. The development of human serum albumin-based drugs and relevant fusion proteins for cancer therapy. *Int. J. Biol. Macromol.* **2021**, *187*, 24−34.
(64) Simard, J. R.; Zunszain, P.; Ha, C.-E.; Yang, J.; Bhagavan, N.; Petitpas, I.; Curry, S.; Hamilton, J. Locating high-affinity fatty acid-binding sites on albumin by x-ray crystallography and NMR spectroscopy. *Proc. Natl. Acad. Sci. U.S.A.* **2005**, *102*, 17958−17963.
(65) De Queiroz, A. A.; Barrak, É. R.; Gil, H. A.; Higa, O. Z. Surface studies of albumin immobilized onto PE and PVC films. *J. Biomater. Sci., Polym. Ed.* **1997**, *8*, 667−681.
(66) De Somer, F.; Van Landschoot, A.; Van Nooten, G.; Delanghe, J. Interaction of plasma proteins with commercial protein repellent polyvinyl chloride (PVC): a word of caution. *Perfusion* **2008**, *23*, 215−221.
(67) Ju, P.; Zhang, Y.; Zheng, Y.; Gao, F.; Jiang, F.; Li, J.; Sun, C. Probing the toxic interactions between polyvinyl chloride microplastics and Human Serum Albumin by multispectroscopic techniques. *Sci. Total Environ.* **2020**, *734*, No. 139219.
(68) Ji, J.; Feng, L.; Shen, J.; Barbosa, M. Preparation of albumin preferential surfaces on poly (vinyl chloride) membranes via surface self-segregation. *J. Biomed. Mater. Res.* **2002**, *61*, 252−259.

(69) Guex, N.; Peitsch, M. C. SWISS-MODEL and the Swiss-Pdb Viewer: an environment for comparative protein modeling. *J. Electrophor.* **1997**, *18*, 2714−2723.
(70) Zhao, D.; Li, L.; He, D.; Zhou, J. Molecular dynamics simulations of conformation changes of HIV-1 regulatory protein on graphene. *Appl. Surf. Sci.* **2016**, *377*, 324−334.
(71) Hung, S.-W.; Hsiao, P.-Y.; Lu, M.-C.; Chieng, C.-C. Thermodynamic investigations using molecular dynamics simulations with potential of mean force calculations for cardiotoxin protein adsorption on mixed self-assembled monolayers. *J. Phys. Chem. B* **2012**, *116*, 12661−12668.
(72) Ross, P. D.; Subramanian, S. Thermodynamics of protein association reactions: forces contributing to stability. *J. Biochem.* **1981**, *20*, 3096−3102.
(73) Paul, T. J.; Parac-Vogt, T. N.; Quiñonero, D.; Prabhakar, R. Investigating polyoxometalate−protein interactions at chemically distinct binding sites. *J. Phys. Chem. B* **2018**, *122*, 7219−7232.
(74) Yang, W.; Yang, L.; Yi, Z.; Wu, Z.; Nie, J.; Zhang, A. Investigating the affinity of BDE154 and 3OH-BDE154 with HSA: Experimental and simulation validation. *Environ. Toxicol. Pharmacol.* **2017**, *51*, 85−93.
(75) Zhang, G.; Keita, B.; Brochon, J.-C.; de Oliveira, P.; Nadjo, L.; Craescu, C. T.; Miron, S. Molecular interaction and energy transfer between human serum albumin and polyoxometalates. *J. Phys. Chem. B* **2007**, *111*, 1809−1814.

https://doi.org/10.1021/acsomega.4c05044
ACS Omega 2024, 9, 38054−38065